energy&fuels

pubs.acs.org/EF

Article

# Antimonene Allotropes $\alpha$- and $\beta$-Phases as Promising Anchoring Materials for Lithium−Sulfur Batteries

Deobrat Singh,* Sanjeev K. Gupta,* Tanveer Hussain, Yogesh Sonvane, P. N. Gajjar, and Rajeev Ahuja*

Cite This: *Energy Fuels* 2021, 35, 9001−9009

Read Online

ACCESS | Metrics & More | Article Recommendations | Supporting Information

**ABSTRACT:** In a quest to mitigate the undesirable shuttling effect that hampers the performance of Li−S batteries, we adopted first-principles calculations to study the anchoring mechanism of lithium polysulfides on antimonene phases, i.e., $\alpha$-Sb and $\beta$-Sb. The anchoring mechanisms of LiPSs on $\alpha$-Sb and $\beta$-Sb were studied through calculations of binding energy, charge transfer, and vertical binding distances from the monolayer to LiPSs. The results indicated that pristine $\alpha$-Sb and $\beta$-Sb showed significant physisorption/chemisorption interactions toward LiPSs due to the considerable $E_b$ values (0.71−1.68 and 0.96−2.07 eV, respectively). Meanwhile, with single Sb vacancy, the binding strength was enhanced (0.83−2.91 eV) for the $\beta$-Sb monolayer. Furthermore, we substituted the Sb atom with the Sn/Te atom and found stronger $E_b$ (1.32−5.69 and 0.45−4.81 eV). All these bindings of LiPSs were much stronger than their interactions with those of electrolytes (DME/DOL) ($E_b$ values: 0.20−1.16 and 0.17−1.07 eV). Also, we investigated the redistribution of electrons and the influence of electronic states near the Fermi level in DOS for LiPSs on $\alpha$-Sb and $\beta$-Sb. Our findings suggest that pristine and defected $\beta$-Sb monolayers could be an excellent anchoring material for Li−S batteries.

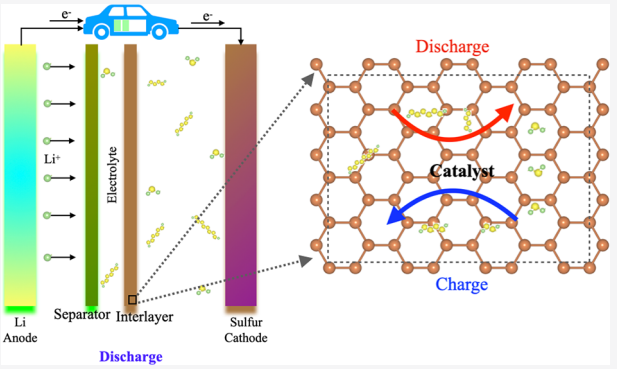


## INTRODUCTION

Finding electrochemical energy storage systems having high energy densities, long lives, reduced masses, and smaller sizes along with environmental compatibility, cost-effectiveness, and worldwide consumer allocation has been an outstanding problem.[1−6] Alkali ion batteries, especially lithium-ion batteries (LIBs), are in high demand due to their intriguing structural and chemical features. It is well known that graphite, which is made up of graphene layers stacked together, has been extensively used as an electrode material in LIBs. Due to the larger contact area between the electrolyte and electrode, it is necessary to improve energy density and increase surface-to-volume ratio, which is highly in demand.[7−10] However, despite having a well-developed technology, metal-ion (Li-ion) batteries are hampered with low energy density and therefore are unable to cope with the soaring demands for energy.

Li−S batteries have established much interest over the past few years, and enhancing the performance of this class of batteries by emerging suitable anchoring materials is a great challenge.[10−15] Sulfur exists in large quantities in nature, having advantages like cost-effectiveness and less toxicity, motivating researchers to utilize it as a cathode in future rechargeable batteries.[15] However, the application of Li−S batteries has been hindered by several reasons: (i) a drop in lithium anode capacity and poor Coulombic efficiency because LiPSs dissolve in commercial organic electrolyte solvents; (ii) limiting the rate performance of the batteries because of the poor ionic/electronic conductivity of sulfur; and (iii) a large volumetric expansion of sulfur (∼80%) during lithiation from the conductive scaffold.[10] Therefore, the most important limiting factor to enhancing the performance of Li−S batteries is by using highly ordered LiPSs. Therefore, innovating efficient ways to trap LiPSs has been one of the important challenges for the realistic application of Li−S batteries.[1,2,5,6,16]

Recently, enormous efforts have been made to settle the abovementioned problems. Due to the quantum confinement effect, various 2D materials[17−19] have been investigated to anchor LiPSs, such as graphene, borophene, phosphorene, silicene, metal oxides, sulfides, MXene, etc.[20−23] Other than graphene, analogues have brought about the investigations of an assortment of materials extending from transition metal dichalcogenides (for example, $MoS_2$, $MoO_3$, $MoSe_2$, $WS_2$, and $WSe_2$), h-BN, to other essential p-block materials (Si, Ge, As, Al, Sn, Sb, and In).[24−27] Recently, it has been discovered that electrode materials having defects not only anchor LIPSs effectively to inhibit the shuttle effect but also prevent their

Received: February 25, 2021
Revised: April 28, 2021
Published: May 7, 2021







https://doi.org/10.1021/acs.energyfuels.1c00607
*Energy Fuels* 2021, 35, 9001−9009

circulation structure from breaking down. Further, defect-induced electrode materials can also expose more active sites for highly efficient sulfur capture and accumulation and dynamically promote its redox reaction.[28,29] The interesting features in structural defects such as vacancies, heteroatoms, chemical functionalizations, and interlayers in materials are probable to be promising anchor sites for LIPSs, consequently preventing the shuttle effect and enhancing the retention capacity of Li−S batteries.[30−34]

Antimonene allotropes, $\alpha$- and $\beta$-phases, displayed semiconducting behaviors with outstanding structural stability verified by phonon dispersion spectra, mechanically and thermally.[35−37] Both $\alpha$-Sb and $\beta$-Sb monolayers were also reported as excellent candidates for ultraviolet optical nanodevices.[38,39] The antimonene monolayers show good potential for LIBs and sodium-ion batteries.[40] In addition, $\alpha$-Sb and $\beta$-Sb monolayers have been successfully synthesized experimentally by several approaches.[41−47] Apart from these, antimonene monolayers have been explored for various other practical applications.[42,48−51] Motivated by these fascinating properties of free-standing pristine antimonene monolayer materials, we have focused on their applications as anchoring materials for Li−S batteries. We studied the structural and electronic properties of pure and defect-induced $\alpha$-Sb and $\beta$-Sb monolayers by DFT calculations. Moreover, the binding energies of different LiPSs at different orientations and active sites on $\alpha$-Sb and $\beta$-Sb surfaces were calculated. Also, the physical/chemical interactions of LiPSs with organic liquid electrolytes DOL/DME were investigated for comparison. Further, to check the effect of LiPSs on the surface of $\alpha$-Sb and $\beta$-Sb monolayers, we have investigated the electronic density of states (DOS) and charge transfer mechanism. To enhance the binding strength of LiPSs on the surface of the Sb monolayer, we considered the vacancy and foreign atom substitution in Sb monolayers.

**Computational Methods.** The DFT framework was performed throughout this project as implemented in the VASP code.[52] For the exchange−correlation functional, the generalized gradient approximation (GGA) within Perdew−Burke−Ernzerhof (PBE) was used. The projector augmented wave (PAW) pseudopotentials in the form of plane-wave basis set were used.[53] The cutoff energy has been set as 500 eV. The electronic structures were fully relaxed until the force on each atom was less than $10^{-3}$ eV/Å. The Monkhorst-Pack (MP) grids[54] used for irreducible Brillouin zone (BZ) sampling were a $(20 \times 20 \times 1)$ $K$-point for the pristine Sb monolayer and $(5 \times 5 \times 1)$ $K$-point for $(3 \times 3 \times 1)$ and $(3 \times 4 \times 1)$ supercell $\alpha$-Sb and $\beta$-Sb monolayers, respectively. The Li anode was oxidized by the discharge process. The electrons shift over an external thread to the cathode, and the Li ion moves toward the cathode through a porous separator. Then, it reacts together with different sulfur concentrations to form $Li_2S_n$ ($n$ = 1, 2, 4, 6, and 8) polysulfides. The adsorption energies of $S_8$/$Li_2S_n$ molecules, $E_{ads}$ or $E_b$, are defined as

$$E_{ads} = E_{Substrate} + E_{S_8/Li_2Sn} - E_{Substrate+S_8/Li_2Sn} \quad (1)$$

where $E_{Substrate}$ is the total energy of pristine and defected $\alpha$-Sb and $\beta$-Sb monolayers, $E_{S_8/Li_2Sn}$ is the total energy of isolated $S_8$/$Li_2S_n$ molecules, and $E_{Substrate + S_8/Li_2Sn}$ is the total energy of the absorbed state on the surface of the Sb monolayer with LiPS molecules. By definition, $E_{ads} > 0$ signifies repulsion among interacting species, and as a result, there is no adsorption. Meanwhile, a negative value $E_b$ shows attraction, which indicates that the adsorption site is favorable as well as stable. Visualization structural analysis (VESTA) was used for all further calculations and analyses including the output structure.[55] To incorporate the long-range interaction in the system, the van der Waals correction scheme of the Grimme (DFT-D3)[56] was applied for geometry optimization and $S_8$/$Li_2S_n$ molecule adsorption.

## RESULTS AND DISCUSSION

**Structural and Electronic Properties.** First, we optimized the structures of antimonene allotropes with two phases $\alpha$-Sb and $\beta$-Sb monolayers, as presented in Figure 1a,b. Both

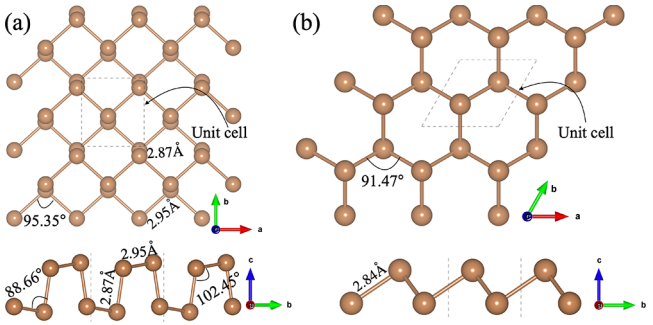


**Figure 1.** Top and side views of optimized structures of (a) $\alpha$-Sb and (b) $\beta$-Sb.

$\alpha$-Sb and $\beta$-Sb monolayers have nonplanar structures. The calculated structural parameters are $a$ = 4.74 Å and $b$ = 4.36 Å, and the corresponding bond lengths between Sb−Sb are 2.95 and 2.87 Å for $\alpha$-Sb, which is presented in Figure 1a. Meanwhile, the lattice parameter of the $\beta$-Sb monolayer is $a$ = $b$ = 4.07 Å and the bond length between Sb−Sb is found to be 2.84 Å. The calculated values of lattice parameters and bond lengths are consistent with previously reported works.[35,38] In addition, each antimony (Sb) atom in the antimonene system is identical with threefold bonds in both phases. Due to different atomic arrangements in the $\alpha$-Sb monolayer, it has three different angles between Sb atoms, as shown in Figure 1a. However, in the case of $\beta$-Sb, the monolayer has hexagonal arrangement due to the fact that it has the same angle (91.47°) between Sb atoms (see Figure 1b).

The electronic band structures are calculated to understand the nature of electronic properties, as shown in Figure 2. The $\alpha$-Sb monolayer shows a semiconducting behavior with band gaps of 0.18 eV (see Figure 2a) and 0.25 eV with PBE and HSE06, respectively. Meanwhile, the $\beta$-Sb monolayer shows band gaps of 1.37 and 1.99 eV with PBE and HSE06, respectively (see Figure 2b). The $\alpha$-Sb monolayer is a direct gap semiconductor between the X and Γ points, while the $\beta$-Sb monolayer has an indirect band gap between the Γ and M points, as presented in Figure 2a,b, which is in agreement with the available literature.[35,38,47] Also, we have investigated the PDOS, as presented in Figure 2c,d. Figure 2c shows that states of Sb 5p orbitals dominate the VBM and CBM, whereas the deep energy of the valence band is derived from the states of 5s orbitals in the case of the $\alpha$-Sb monolayer. Similar orbital contributions are found in the $\beta$-Sb, in which the VBM and CBM are made by 5p orbitals, as presented in Figure 2d.

**Adsorption of LiPSs on $\alpha$- and $\beta$-Sb Monolayers.** Usually, during the discharging process in Li−S batteries, the


https://doi.org/10.1021/acs.energyfuels.1c00607
Energy Fuels 2021, 35, 9001−9009

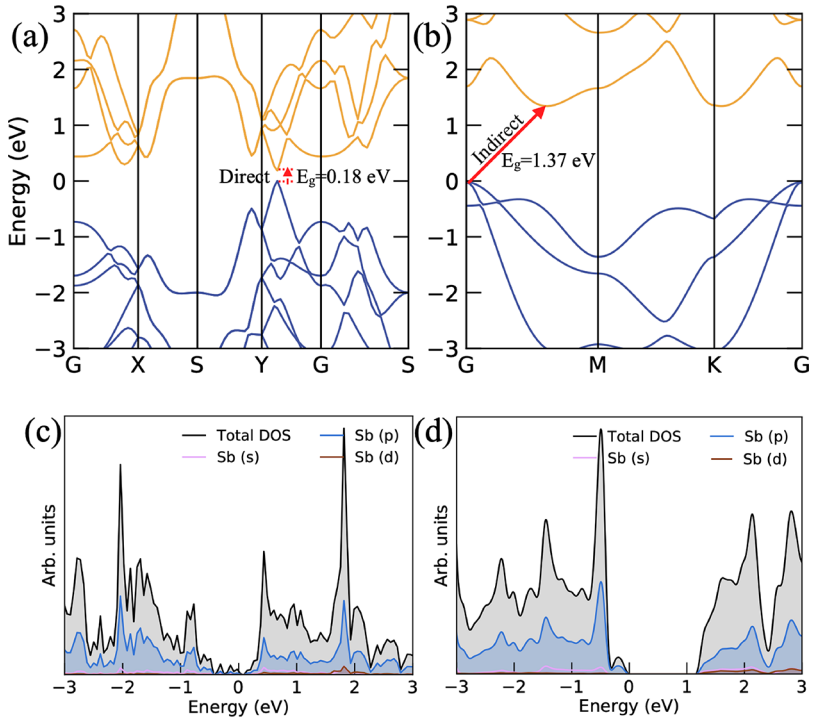


**Figure 2.** (a, b) Electronic band structures of $\alpha$-Sb and $\beta$-Sb and (c, d) corresponding projected densities of states (PDOS) of $\alpha$-Sb and $\beta$-Sb, respectively.

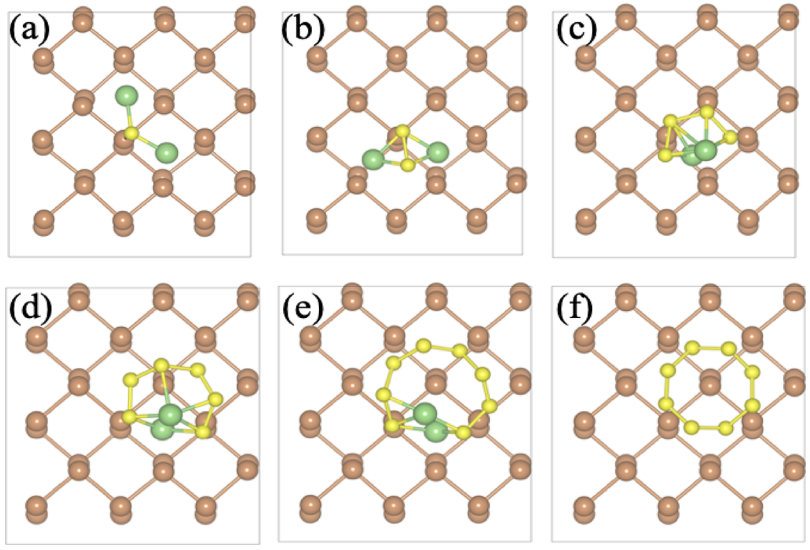


**Figure 3.** Optimized structures of pristine $\alpha$-Sb with the PBE functional for (a) $Li_2S$@Sb, (b) $Li_2S_2$@Sb, (c) $Li_2S_4$@Sb, (d) $Li_2S_6$@Sb, (e) $Li_2S_8$@Sb, and (f) $S_8$@Sb.

lithium ions decompose from the anode and interact with the sulfur cathode to form the LiPSs, such as $Li_2S_8$, $Li_2S_6$, $Li_2S_4$, $Li_2S_2$, and $Li_2S$, as demonstrated by theoretical and experimental studies.[57−59] Before proceeding to a detailed investigation of $\alpha$-Sb and $\beta$-Sb monolayers as cathodic anchoring materials for Li−S batteries, it is interesting to first optimize these LiPSs. The variation of bond length in $S_8$ and $Li_2S_n$ ($n$ = 1, 2, 4, 6, and 8) between Li−S and S−S bonds is presented in Figure S1. It is evident that the length of the Li−S bonds decreases with the decrease in the concentration of sulfur in the $Li_2S_n$ cluster ($n$ = 1, 2, 4, 6, and 8), while the S−S bonds vary depending on the number of sulfur atoms, which indicates that $Li_2S_n$ chain species ($n$ = 4, 6, and 8) are easier to ionize in Li cations and polysulfide anions in the electrolyte than $Li_2S_2$ or $Li_2S$, which is consistent with the literature.[60]

Now, we have explored the interaction of LiPS species with $\alpha$-Sb and $\beta$-Sb monolayers. We have considered all the possible orientations of LiPSs on the surface of $\alpha$-Sb and $\beta$-Sb monolayers, and the most stable configurations are shown in Figures 3 and 4. After the structures are optimized, the vertical distance between $\alpha$-Sb and $\beta$-Sb surfaces and LiPS species are more than 2.0 Å. In the case of long chain $Li_2S_n$ ($n$ = 4, 6, and 8), the lithium atoms are shifted at the hollow side of the hexagonal arrangement of $\alpha$-Sb and $\beta$-Sb surfaces and sulfur atoms are oriented to be parallel to the antimonene monolayer.



https://doi.org/10.1021/acs.energyfuels.1c00607
Energy Fuels 2021, 35, 9001−9009

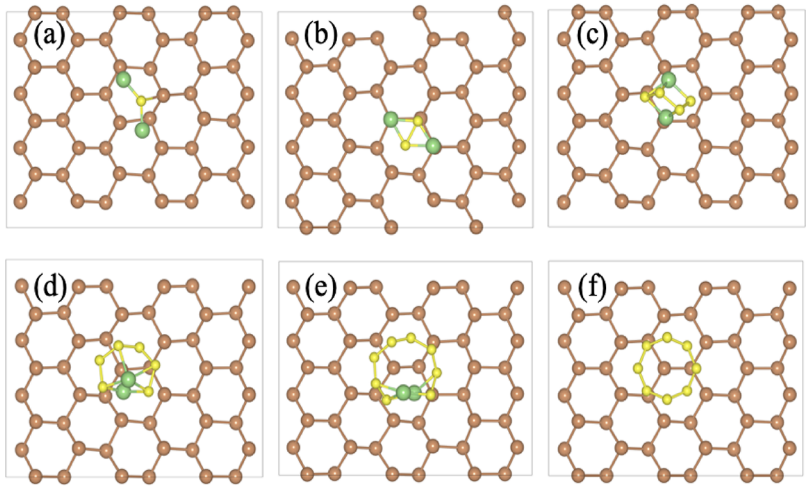


**Figure 4.** Optimized structures of pristine $\beta$-Sb with the PBE functional for (a) $Li_2S$@Sb, (b) $Li_2S_2$@Sb, (c) $Li_2S_4$@Sb, (d) $Li_2S_6$@Sb, (e) $Li_2S_8$@Sb, and (f) $S_8$@Sb.

However, in the case of short chain $Li_2S_n$ ($n$ = 1 and 2), the lithium atoms are slightly displaced from the hexagonal arrangement of antimony atoms in $\alpha$-Sb and $\beta$-Sb surfaces due to the restriction of bonds between lithium and sulfur atoms. Additionally, the Li atoms bonded with the Sb atoms of $\alpha$-Sb and $\beta$-Sb surfaces with a bond length of 2.83 Å and Sb to S bond length (which is located just above the Sb atom) is found to be 2.58 Å in short chain $Li_2S$ species, as shown in Figure 3a. Also, bond lengths between the $Li_2S_2$ species and antimonene surface are 2.83 and 2.99 Å for Sb−Li and Sb−S, respectively (for pristine $\alpha$-Sb, as shown in Figure 3). The vertical distance between $\alpha$-Sb and $\beta$-Sb surfaces to LiPS species varies from 1.98 to 2.81 Å (see Table 1) for pristine $\alpha$-Sb and $\beta$-Sb.

**Table 1. Calculated Binding Energy [eV], Charge Transfer Mechanism Calculated by Bader Charge Analysis, and Corresponding Vertical Distance ($d$) from the Surface of Sb to LiPS Molecules**

| | binding energy [eV] | | Bader charge [e] | | $d$ [Å] | |
|---|---|---|---|---|---|---|
| systems/LiPSs | $\alpha$-Sb | $\beta$-Sb | $\alpha$-Sb | $\beta$-Sb | $\alpha$-Sb | $\beta$-Sb |
| $Li_2S$ | 1.68 | 2.07 | 0.15 | 0.51 | 2.03 | 2.04 |
| $Li_2S_2$ | 1.17 | 1.35 | 0.44 | 0.32 | 2.23 | 2.23 |
| $Li_2S_4$ | 0.98 | 1.01 | 0.15 | 0.10 | 2.32 | 2.15 |
| $Li_2S_6$ | 0.88 | 1.164 | 0.13 | 0.06 | 2.15 | 2.03 |
| $Li_2S_8$ | 1.11 | 1.40 | 0.06 | 0.01 | 2.13 | 1.98 |
| $S_8$ | 0.71 | 0.96 | −0.15 | 0.08 | 2.81 | 2.67 |

**Adsorption of LiPSs on Defected Antimonene Monolayers.** Furthermore, we have studied the single Sb vacancy from the pristine $\beta$-Sb phase due to the significantly better binding strength than the pristine $\alpha$-Sb phase. Similar trends are found in the defected antimonene surface, as shown in Figure 5a−f. For $Li_2S$ species, the lithium atoms shifted toward the Sb vacancy site and made a hexagonal arrangement with the combination of Sb atoms. The bond length between Sb and Li atoms is 2.83 Å, the same as the pristine case, and the Sb to S bond length is 2.45 Å, which is shorter than the pristine case. In the case of the single Sb vacancy system, vertical distance varies from 1.20 to 2.33 Å (see in Table 2).

Moreover, we have further modified the antimonene monolayer surface by substituting a single Sb atom with V and VI group atoms, just the left and right atoms of Sb in the periodic table. The V group atoms (Sn) are one-electron-deficient, while VI group atoms (Te) are rich by one electron, thus making the systems both p-type/n-type, respectively. This modification of the antimonene surfaces significantly changes the binding strength of LiPSs. The calculated $E_b$ values are −3.71 and −4.32 eV for Sn- and Te-doped systems in the $\beta$-Sb phase of the antimonene monolayer. The negative $E_b$ represents that the Sn- and Te-doped systems are energetically more favorable (see Figure S2). The most preferential absorption sites are shown in Figures S3 and S4 for each LiPS species on the surface of the $\beta$-Sb phase with Sn- and Te-defected cases, respectively. After relaxation, the LiPS species shifted more than 1.5 Å away from the antimonene surface.

In the case of $Li_2S$ species, the bond lengths between Li−Sb and S−Sb are 2.46 and 3.17 Å, respectively, in which Li−Sb bond length decreases and S−Sb bond length increases, as compared to the cases without the dopant. Additionally, for long chain $Li_2S_n$ ($n$ = 2, 4, 6, and 8), each species shifted in an upward direction to the antimonene surface, as presented in Table 2. Additionally, species of LiPS are distorted to some degree when adsorbed on these substrates. It was seen that the variation of bond length of these adsorbed systems is less in S−S bonds and Li−S bonds as they are elongated. It is also seen that in the short chain $Li_2S_n$, i.e., $n$ = 1 and 2, the bond length variation in Li−S is larger than that in long chain $Li_2S_n$, i.e., $n$ = 4, 6, and 8. This is because long chain LiPSs have more chemical bonds in Li and S atoms, which makes elongation difficult.

To investigate the anchoring performance, we have calculated the $E_b$ of different groups of $Li_2S_n$ ($n$ = 1, 2, 4, 6, and 8) and $S_8$ in $\alpha$-Sb and $\beta$-Sb (see in Figure 6). As shown in Figure 6b, the $E_b$ values on pristine antimonene with $\alpha$-Sb ($\beta$-Sb) are 1.68 (2.07) eV, 1.17 (1.35) eV, 0.98 (1.01) eV, 0.88 (1.16) eV, 1.11 (1.40) eV, and 0.71 (0.96) eV for $Li_2S_n$ ($n$ = 1, 2, 4, 6, and 8) and $S_8$, respectively. The $\beta$-Sb monolayer has better anchoring performance than $\alpha$-Sb. This is the reason we further considered the $\beta$-Sb monolayer as an anchoring material for Li−S batteries. The $E_b$ is 0.96 eV for $S_8$, increases up to 1.40 eV for $Li_2S_8$, and further steadily decreases up to 1.01 eV for $Li_2S_4$. Also, in the case of $Li_2S_2$ and $Li_2S$, the $E_b$


https://doi.org/10.1021/acs.energyfuels.1c00607
Energy Fuels 2021, 35, 9001−9009

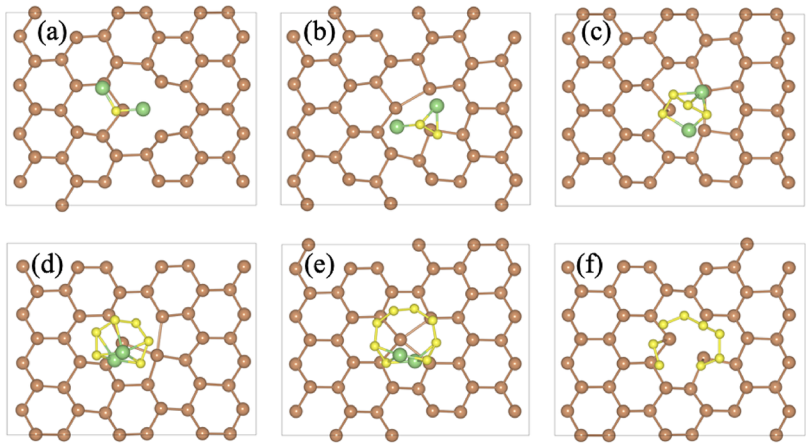


**Figure 5.** Optimized structures of single Sb vacancy in $\beta$-Sb with the PBE functional for (a) $Li_2S$@Sb, (b) $Li_2S_2$@Sb, (c) $Li_2S_4$@Sb, (d) $Li_2S_6$@Sb, (e) $Li_2S_8$@Sb, and (f) $S_8$@Sb.

**Table 2. Calculated Binding Energy [eV], Charge Transfer Mechanism Calculated by Bader Charge Analysis, and Corresponding Vertical Distance ($d$) from the Surface of Defected $\beta$-Sb to LiPS Molecules**

| | binding energy [eV] | | Bader charge [e] | | $d$ [Å] | |
|---|---|---|---|---|---|---|
| systems/LiPSs | $\beta$-$Sb_V$ | $\beta$-$Sb_{D(Sn/Te)}$ | $\beta$-Sb | $\beta$-$Sb_{D(Sn/Te)}$ | $\beta$-Sb | $\beta$-$Sb_{D(Sn/Te)}$ |
| $Li_2S$ | 2.91 | 5.44/4.81 | 0.12 | 0.30/0.42 | 1.20 | 1.48/1.63 |
| $Li_2S_2$ | 1.84 | 5.64/4.20 | 0.10 | 0.52/0.23 | 1.19 | 1.64/1.80 |
| $Li_2S_4$ | 1.27 | 5.69/2.44 | 0.03 | 0.24/0.16 | 1.50 | 1.62/2.32 |
| $Li_2S_6$ | 0.88 | 5.17/4.00 | 0.08 | 0.25/0.24 | 2.01 | 1.65/1.55 |
| $Li_2S_8$ | 1.08 | 5.32/4.20 | 0.02 | 0.25/0.23 | 2.25 | 1.92/1.79 |
| $S_8$ | 0.83 | 1.32/0.45 | 0.01 | 0.10/0.08 | 2.33 | 2.59/2.73 |

slightly increases and is found to be 1.35 and 2.07 eV, as displayed in Table 1, which presented similarity in the case of the $\alpha$-Sb monolayer. Furthermore, for single Sb atom vacancy in $\beta$-Sb, the $E_b$ for $S_8$ is 0.83 eV, and the interaction becomes slightly lower and influences the strongest interactions with a value of 2.91 eV in the final stage ($Li_2S$), which is noticeably greater than that of $Li_2S_n$ species with the pristine $\alpha$-Sb and $\beta$-Sb phases of the antimonene monolayer.

Moreover, we further enhance the binding strength of LiPS species with substrates as compared to LiPSs with organic solvents by substituting Sn and Te atoms in place of single antimony atoms in the $\beta$-Sb monolayer for excellent performance of anchoring materials for Li−S batteries. When we replaced single Sb atoms and heteroatoms with Sn/Te, then the $\beta$-Sb monolayer surface losses/gains one electron due to the fact that the interactions between LiPS species and the defected $\beta$-Sb surface are significantly enhanced. According to that, the binding strengths are significantly enhanced as compared to the previously discussed system. The binding energies vary from 1.32 to 5.69 eV and 0.45 to 4.81 eV for Sn- and Te-substituted atoms in the $\beta$-Sb surface for $S_8$ and $Li_2S_n$ ($n$ = 1, 2, 4, 6, and 8) species (see in Table 2), which is better than the previously reported works.[30,34,61−67] These binding strengths suggest that the defective $\beta$-Sb surface is an excellent material that can effectively anchor the LiPS soluble groups because of the greater binding strength.

**Charge Transfer Mechanism, Electrical Conductivity, and Interactions of LiPSs with Organic Electrolytes.** We have investigated the charge transfer between the LiPSs and antimonene surface. The number of charges transferred in different configurations of antimonene during the sulfur-containing lithium process has been presented and is shown in Figure 7 (also see Tables 1 and 2). The charge transferred into the $S_n$-substituted antimonene monolayer ($\Delta Q$) can be found to be the largest in the entire process, leading to strong binding energy and an enhanced anchoring effect. Meanwhile, for Sb vacancy in $\beta$-Sb, hardly any electron is transferred between the groups ($S_8$ and $Li_2S_8$) and the antimonene substrate, where the anchoring is due to vdW interaction. Overall, we can see that the significant charge transfer mechanism occurs due to the strong interaction between the LiPS species and antimonene substrate, while single substitutional Sb atoms have more charge transfer, which supports stronger binding strength.

To check the charge transfer mechanism between the LiPS species and Sb monolayer, the work function has been investigated for Sn and Te substitute atoms in the $\beta$-Sb system. The calculated work functions are 4.5 and 3.79 eV for Sn and Te substitute atoms in the $\beta$-Sb monolayer, respectively, which is lower than the pristine $\beta$-Sb monolayer (4.87 eV). In the case of Sn, the electron-deficient property of the Sn atom leads to the Fermi level to shift downward, while the electron-rich Te atom causes the Fermi level to shift upward in $\beta$-antimonene. It is also shown that the Sn-doped system displayed p-type behavior, while the Te-doped system exhibited n-type behavior in comparison with pristine antimonene (see Figures S5 and S6 in the Supporting Information). As a result, each species of the LiPSs and $S_8$ donates more electrons to the $S_n$ defected antimonene when they are absorbed into the substrate, resulting in strong interaction. It was also seen that the Li−S batteries have low-electrical-conductivity sulfur and reducing products. Therefore, the conductivity of the systems adsorbing LiPS species is significantly important. Figures S7 and S8 in the Supporting


https://doi.org/10.1021/acs.energyfuels.1c00607
Energy Fuels 2021, 35, 9001−9009

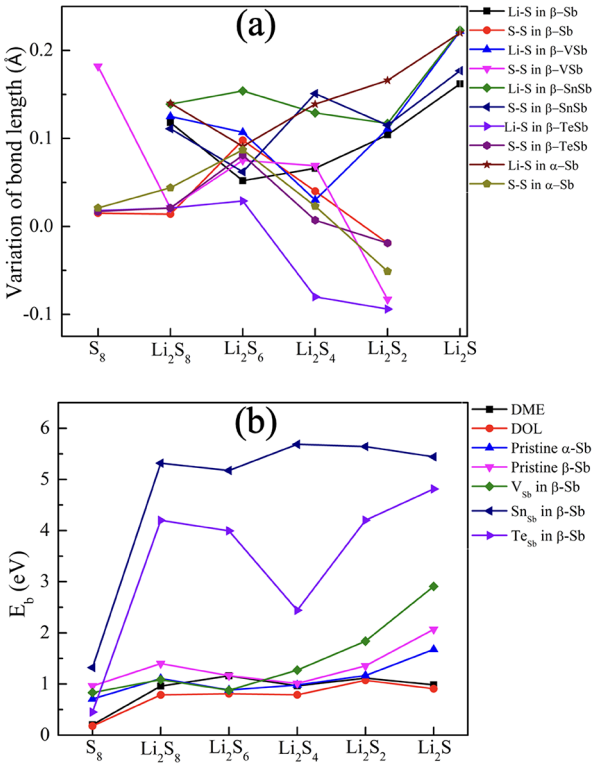


**Figure 6.** (a) Variations of bond length between Li−S and S−S after adsorption on the surface of $\alpha$-Sb and $\beta$-Sb monolayers with pristine and defected systems. (b) Binding energies $E_b$ (eV) of $S_8$ and $Li_2S_n$ ($n$ = 1, 2, 4, 6, and 8) clusters on the surface of $\alpha$-Sb and $\beta$-Sb monolayers with pristine and defected systems. For comparison of binding strengths of LiPSs with substrates and electrolytes (DME and DOL) with LiPS species.

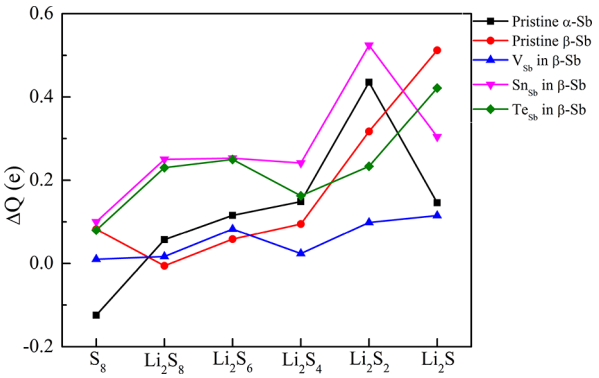


**Figure 7.** Charge transfer mechanism between the adsorbed LiPS cluster and antimonene monolayer.

Information show the decomposed DOS before and after the adsorption of LiPS species. Despite the fact that the pristine antimonene shows a semiconducting behavior, it is reduced by adsorbing LiPS species. From the relation of $E_g$ and electrical conductivity ($\sigma \approx \exp(-E_g/K_BT)$),[68] the narrow band gap enhanced the electrical conductivity of the antimonene substrate after the absorption of LiPS species, which will considerably improve the Li−S batteries' performance.

Last, we have calculated the structural properties of LiPSs and 1,3-dioxolane electrolyte molecules (DOL)/dimethyl ether (DME), as shown in Figure S1 (in the Supporting Information). We have calculated the binding strength of these two liquid organic electrolytes DOL and DME with the LiPS cluster for the sake of comparison with those of $\alpha$-Sb and $\beta$-Sb substrates. The $E_b$ values of LiPSs with the considered electrolytes were calculated by

$$E_b = E_{LIPSs} + E_{DOS/DME} - E_{LiPSs+DOL/DME} \quad (2)$$

where $E_{LiPSs + DOL/DME}$, $E_{LIPSs}$, and $E_{DOS/DME}$ represent the total energies of the electrolytes with LiPSs, the isolated LiPS cluster, and the electrolyte molecule, respectively. On the other hand, it is shown that DOL and DME have nearly similar $E_b$ values for LiPSs of 0.78−1.07 and 0.95−1.16 eV, respectively. From the above discussion, the $E_b$ values of LiPSs with electrolytes (see Figure S9 and Table S1 in the Supporting Information) are smaller than those with the $\alpha$-Sb monolayer for each step of the reduction of LiPSs, except $Li_2S_6$, while in the case of the $\beta$-Sb monolayer, LiPSs have overall larger binding energies than LiPSs with electrolytes. It can be concluded from the results that LiPSs are anchored in the $\beta$-Sb monolayer and do not dissolve in the electrolyte from an energetic point of view. Also, the $E_b$ values of $Li_2S_n$ with electrolytes are smaller than those of $Li_2S_n$ with single Sb vacancy in the $\beta$-Sb monolayer, except $Li_2S_6$ species. As a result, the examined $\beta$-Sb monolayers can effectively suppress the shuttle effect.[69,70] In addition, we also examined the defective antimonene monolayer, which significantly improved the $E_b$ of LiPSs with the substrate and has larger $E_b$ than LiPSs with electrolytes, so that the doped system could be a superior anchoring material for Li−S batteries.

## CONCLUSIONS

We have investigated the lithiation process and fully analyzed the anchoring effect of antimonene allotropes with $\alpha$-Sb and $\beta$-Sb layered-structured materials. The $\alpha$- and $\beta$-antimonene displayed a distinct adsorption mechanism with LiPS clusters, where the $E_b$ is computed by the values of charge transfer from the S-containing cluster to the Sb surface. The anchoring effect is described by softening of Li−S bonds, while the destruction of LiPS clusters is signified by strong binding strength. On the basis of this, Sb monolayer materials can induce remarkable changes with sufficient binding strengths of 1.32−5.69/0.45−4.81 eV for Sn/Te-doped antimonene monolayers to have physisorption interaction during the lithiation stage. Moreover, the interaction of LiPS species avoids dissolution in the electrolyte. The investigated results propose that antimonene can be a promising anchoring material for Li−S batteries for cathode materials, which provides theoretical evidence for the investigated layered materials for the further progress of battery performance.

## ASSOCIATED CONTENT

### Supporting Information

The Supporting Information is available free of charge at https://pubs.acs.org/doi/10.1021/acs.energyfuels.1c00607.

Optimized structures of lithium polysulfides (LiPSs), organic electrolytes, and Sn/Te adatoms in the $\beta$-Sb monolayer, adsorptions of LiPSs on the $\beta$-Sb monolayer, interaction of organic electrolytes with LiPS molecules, and electronic density of states (PDF)



https://doi.org/10.1021/acs.energyfuels.1c00607
Energy Fuels 2021, 35, 9001−9009

## AUTHOR INFORMATION


### Corresponding Authors

**Deobrat Singh** − *Condensed Matter Theory Group, Department of Physics and Astronomy, Uppsala University, S-75120 Uppsala, Sweden;* orcid.org/0000-0001-7246-8743; Email: deobrat.singh@physics.uu.se

**Sanjeev K. Gupta** − *Computational Materials and Nanoscience Group, Department of Physics and Electronics, St. Xavier's College, Ahmedabad 380009, India;* orcid.org/0000-0002-3060-2104; Email: sanjeev.gupta@sxca.edu.in

**Rajeev Ahuja** − *Condensed Matter Theory Group, Department of Physics and Astronomy, Uppsala University, S-75120 Uppsala, Sweden; Department of Physics, Indian Institute of Technology Ropar, Rupnagar 140001, Punjab, India;* orcid.org/0000-0003-1231-9994; Email: rajeev.ahuja@physics.uu.se

### Authors

**Tanveer Hussain** − *School of Molecular Sciences, The University of Western Australia, Perth, WA 6009, Australia; School of Chemical Engineering, The University of Queensland, St Lucia, Brisbane 4072, Australia;* orcid.org/0000-0002-0300-0503

**Yogesh Sonvane** − *Applied Materials Lab, Department of Physics, Sardar Vallabhbhai National Institute of Technology, Surat 395007, India;* orcid.org/0000-0001-7319-2865

**P. N. Gajjar** − *Department of Physics, University School of Sciences, Gujarat University, Ahmedabad 380009, India*

Complete contact information is available at: https://pubs.acs.org/10.1021/acs.energyfuels.1c00607


### Notes

The authors declare no competing financial interest.

## ACKNOWLEDGMENTS

D.S. and R.A. thank Olle Engkvists Stiftelse (198-0390), Carl Tryggers Stiftelse for Vetenskaplig Forskning (CTS: 18:4), and Swedish Research Council (VR-2016-06014 and VR-2020-04410) for financial support. S.K.G. would like to thank the Science and Engineering Research Board (SERB), India, for the financial support (grant no.: YSS/2015/001269). P.N.G. is thankful to the Department of Science and Technology, India, for the support under DST-FIST and the University Grants Commission, India, for the support under DRS-SAP. SNIC and HPC2N are acknowledged for providing the computing facilities.

## REFERENCES


(1) Zhu, K.; Wang, C.; Chi, Z.; Ke, F.; Yang, Y.; Wang, A.; Wang, W.; Miao, L. How Far Away Are Lithium-Sulfur Batteries From Commercialization? *Front. Energy Res.* **2019**, *7*, 123.

(2) Li, Z.; He, Q.; Xu, X.; Zhao, Y.; Liu, X.; Zhou, C.; Ai, D.; Xia, L.; Mai, L. A 3D Nitrogen-Doped Graphene/TiN Nanowires Composite as a Strong Polysulfide Anchor for Lithium-Sulfur Batteries with Enhanced Rate Performance and High Areal Capacity. *Adv. Mater.* **2018**, *30*, 1804089.

(3) Sun, Z.; Zhang, J.; Yin, L.; Hu, G.; Fang, R.; Cheng, H.-M.; Li, F. Conductive Porous Vanadium Nitride/Graphene Composite as Chemical Anchor of Polysulfides for Lithium-Sulfur Batteries. *Nat. Commun.* **2017**, *8*, 14627.

(4) Tan, J.; Liu, D.; Xu, X.; Mai, L. *In Situ* / Operando Characterization Techniques for Rechargeable Lithium−Sulfur Batteries: A Review. *Nanoscale* **2017**, *9*, 19001−19016.

(5) Ji, X.; Lee, K. T.; Nazar, L. F. A Highly Ordered Nanostructured Carbon−Sulphur Cathode for Lithium−Sulphur Batteries. *Nat. Mater.* **2009**, *8*, 500−506.

(6) Manthiram, A.; Fu, Y.; Chung, S.-H.; Zu, C.; Su, Y.-S. Rechargeable Lithium−Sulfur Batteries. *Chem. Rev.* **2014**, *114*, 11751−11787.

(7) Zhang, L.; Yang, X.; Zhang, F.; Long, G.; Zhang, T.; Leng, K.; Zhang, Y.; Huang, Y.; Ma, Y.; Zhang, M.; et al. Controlling the Effective Surface Area and Pore Size Distribution of $Sp^2$ Carbon Materials and Their Impact on the Capacitance Performance of These Materials. *J. Am. Chem. Soc.* **2013**, *135*, 5921−5929.

(8) Lukatskaya, M. R.; Kota, S.; Lin, Z.; Zhao, M.-Q.; Shpigel, N.; Levi, M. D.; Halim, J.; Taberna, P.-L.; Barsoum, M. W.; Simon, P.; et al. Ultra-High-Rate Pseudocapacitive Energy Storage in Two-Dimensional Transition Metal Carbides. *Nat. Energy* **2017**, *2*, 17105.

(9) Zhu, Y.; Murali, S.; Stoller, M. D.; Ganesh, K. J.; Cai, W.; Ferreira, P. J.; Pirkle, A.; Wallace, R. M.; Cychosz, K. A.; Thommes, M.; Su, D.; Stach, E. A.; Ruoff, R. S. Carbon-Based Supercapacitors Produced by Activation of Graphene. *Science* **2011**, *332*, 1537−1541.

(10) Ma, H.; Chen, H.; Wu, M.; Chi, F.; Liu, F.; Bai, J.; Cheng, H.; Li, C.; Qu, L. Maximization of Spatial Charge Density: An Approach to Ultrahigh Energy Density of Capacitive Charge Storage. *Angew. Chem., Int. Ed.* **2020**, *59*, 14541−14549.

(11) Shi, Q. X.; Guan, X.; Pei, H. J.; Chang, C.; Qu, H.; Xie, X. L.; Ye, Y. S. Functional Covalent Triazine Frameworks-Based Quasi-Solid-State Electrolyte Used to Enhance Lithium Metal Battery Safety. *Batteries Supercaps* **2020**, *3*, 936−945.

(12) Chen, L.; Yang, W.; Liu, J.; Zhou, Y. Decorating $CoSe_2$ Hollow Nanospheres on Reduced Graphene Oxide as Advanced Sulfur Host Material for Performance Enhanced Lithium-Sulfur Batteries. *Nano Res.* **2019**, *12*, 2743−2748.

(13) He, Y.; Xiang, K.; Wang, Y.; Zhou, W.; Zhu, Y.; Xiao, L.; Chen, W.; Chen, X.; Chen, H.; Cheng, H.; et al. Scalable and Controllable Synthesis of Multi-Shell Hollow Carbon Microspheres for High-Performance Supercapacitors. *Carbon* **2019**, *154*, 330−341.

(14) Wen, X.; Lu, X.; Xiang, K.; Xiao, L.; Liao, H.; Chen, W.; Zhou, W.; Chen, H. Nitrogen/Sulfur Co-Doped Ordered Carbon Nanoarrays for Superior Sulfur Hosts in Lithium-Sulfur Batteries. *J. Colloid Interface Sci.* **2019**, *554*, 711−721.

(15) Pan, Y.; Chou, S.; Liu, H. K.; Dou, S. X. Functional Membrane Separators for Next-Generation High-Energy Rechargeable Batteries. *Natl. Sci. Rev.* **2017**, *4*, 917−933.

(16) Cai, X.; Lai, L.; Shen, Z.; Lin, J. Graphene and Graphene-Based Composites as Li-Ion Battery Electrode Materials and Their Application in Full Cells. *J. Mater. Chem. A* **2017**, *5*, 15423−15446.

(17) Jana, M.; Xu, R.; Cheng, X.-B.; Yeon, J. S.; Park, J. M.; Huang, J.-Q.; Zhang, Q.; Park, H. S. Rational Design of Two-Dimensional Nanomaterials for Lithium−Sulfur Batteries. *Energy Environ. Sci.* **2020**, *13*, 1049−1075.

(18) Naguib, M.; Kurtoglu, M.; Presser, V.; Lu, J.; Niu, J.; Heon, M.; Hultman, L.; Gogotsi, Y.; Barsoum, M. W. Two-Dimensional Nanocrystals Produced by Exfoliation of $Ti_3AlC_2$. *Adv. Mater.* **2011**, *23*, 4248−4253.

(19) Pang, J.; Mendes, R. G.; Bachmatiuk, A.; Zhao, L.; Ta, H. Q.; Gemming, T.; Liu, H.; Liu, Z.; Rummeli, M. H. Applications of 2D MXenes in Energy Conversion and Storage Systems. *Chem. Soc. Rev.* **2019**, *48*, 72−133.

(20) Shao, Q.; Wu, Z.-S.; Chen, J. Two-Dimensional Materials for Advanced Li-S Batteries. *Energy Storage Mater.* **2019**, *22*, 284−310.

(21) Tang, H.; Li, W.; Pan, L.; Tu, K.; du, F.; Qiu, T.; Yang, J.; Cullen, C. P.; McEvoy, N.; Zhang, C. J. A Robust, Freestanding MXene-Sulfur Conductive Paper for Long-Lifetime Li−S Batteries. *Adv. Funct. Mater.* **2019**, *29*, 1901907.

(22) Cheng, X.-B.; Zhang, R.; Zhao, C.-Z.; Zhang, Q. Toward Safe Lithium Metal Anode in Rechargeable Batteries: A Review. *Chem. Rev.* **2017**, *117*, 10403−10473.

(23) Ali, T.; Yan, C. 2 D Materials for Inhibiting the Shuttle Effect in Advanced Lithium−Sulfur Batteries. *ChemSusChem* **2020**, *13*, 1447−1479.
(24) Eftekhari, A.; Kim, D.-W. Cathode Materials for Lithium−Sulfur Batteries: A Practical Perspective. *J. Mater. Chem. A* **2017**, *5*, 17734−17776.
(25) Fan, Y.; Yang, Z.; Hua, W.; Liu, D.; Tao, T.; Rahman, M. M.; Lei, W.; Huang, S.; Chen, Y. Functionalized Boron Nitride Nanosheets/Graphene Interlayer for Fast and Long-Life Lithium-Sulfur Batteries. *Adv. Energy Mater.* **2017**, *7*, 1602380.
(26) Yuan, Z.; Peng, H.-J.; Hou, T.-Z.; Huang, J.-Q.; Chen, C.-M.; Wang, D.-W.; Cheng, X.-B.; Wei, F.; Zhang, Q. Powering Lithium−Sulfur Battery Performance by Propelling Polysulfide Redox at Sulfiphilic Hosts. *Nano Lett.* **2016**, *16*, 519−527.
(27) Ye, H.; Li, M.; Liu, T.; Li, Y.; Lu, J. Activating $Li_2S$ as the Lithium-Containing Cathode in Lithium−Sulfur Batteries. *ACS Energy Lett.* **2020**, *5*, 2234−2245.
(28) Zhang, Y.; Tao, L.; Xie, C.; Wang, D.; Zou, Y.; Chen, R.; Wang, Y.; Jia, C.; Wang, S. Defect Engineering on Electrode Materials for Rechargeable Batteries. *Adv. Mater.* **2020**, *32*, 1905923.
(29) Liu, H.; Lei, W.; Tong, Z.; Li, X.; Wu, Z.; Jia, Q.; Zhang, S.; Zhang, H. Defect Engineering of 2D Materials for Electrochemical Energy Storage. *Adv. Mater. Interfaces* **2020**, *7*, 2000494.
(30) Zhang, Q.; Wang, Y.; Seh, Z. W.; Fu, Z.; Zhang, R.; Cui, Y. Understanding the Anchoring Effect of Two-Dimensional Layered Materials for Lithium−Sulfur Batteries. *Nano Lett.* **2015**, *15*, 3780−3786.
(31) Li, N.; Meng, Q.; Zhu, X.; Li, Z.; Ma, J.; Huang, C.; Song, J.; Fan, J. Lattice Constant-Dependent Anchoring Effect of MXenes for Lithium−Sulfur (Li−S) Batteries: A DFT Study. *Nanoscale* **2019**, *11*, 8485−8493.
(32) Fang, M.; Liu, X.; Ren, J.-C.; Yang, S.; Su, G.; Fang, Q.; Lai, J.; Li, S.; Liu, W. Revisiting the Anchoring Behavior in Lithium-Sulfur Batteries: Many-Body Effect on the Suppression of Shuttle Effect. *npj Comput. Mater.* **2020**, *6*, 8.
(33) Ye, C.; Chao, D.; Shan, J.; Li, H.; Davey, K.; Qiao, S.-Z. Unveiling the Advances of 2D Materials for Li/Na-S Batteries Experimentally and Theoretically. *Matter* **2020**, *2*, 323−344.
(34) Lin, H.; Yang, D.-D.; Lou, N.; Wang, A.-L.; Zhu, S.-G.; Li, H.-Z. Defect Engineering of Black Phosphorene towards an Enhanced Polysulfide Host and Catalyst for Lithium-Sulfur Batteries: A First Principles Study. *J. Appl. Phys.* **2019**, *125*, No. 094303.
(35) Wang, G.; Pandey, R.; Karna, S. P. Atomically Thin Group V Elemental Films: Theoretical Investigations of Antimonene Allotropes. *ACS Appl. Mater. Interfaces* **2015**, *7*, 11490−11496.
(36) Ares, P.; Palacios, J. J.; Abellán, G.; Gómez-Herrero, J.; Zamora, F. Recent Progress on Antimonene: A New Bidimensional Material. *Adv. Mater.* **2018**, *30*, 1703771.
(37) Kripalani, D. R.; Kistanov, A. A.; Cai, Y.; Xue, M.; Zhou, K. Strain Engineering of Antimonene by a First-Principles Study: Mechanical and Electronic Properties. *Phys. Rev. B* **2018**, *98*, No. 085410.
(38) Singh, D.; Gupta, S. K.; Sonvane, Y.; Lukačević, I. Antimonene: A Monolayer Material for Ultraviolet Optical Nanodevices. *J. Mater. Chem. C* **2016**, *4*, 6386−6390.
(39) Xu, Y.; Peng, B.; Zhang, H.; Shao, H.; Zhang, R.; Zhu, H. First-Principle Calculations of Optical Properties of Monolayer Arsenene and Antimonene Allotropes. *Ann. Phys.* **2017**, *529*, 1600152.
(40) Sengupta, A.; Frauenheim, T. Lithium and Sodium Adsorption Properties of Monolayer Antimonene. *Mater. Today Energy* **2017**, *5*, 347−354.
(41) Ji, J.; Song, X.; Liu, J.; Yan, Z.; Huo, C.; Zhang, S.; Su, M.; Liao, L.; Wang, W.; Ni, Z.; et al. Two-Dimensional Antimonene Single Crystals Grown by van Der Waals Epitaxy. *Nat. Commun.* **2016**, *7*, 13352.
(42) Wang, X.; Song, J.; Qu, J. Antimonene: From Experimental Preparation to Practical Application. *Angew. Chem., Int. Ed.* **2019**, *58*, 1574−1584.
(43) Shao, Y.; Liu, Z.-L.; Cheng, C.; Wu, X.; Liu, H.; Liu, C.; Wang, J.-O.; Zhu, S.-Y.; Wang, Y.-Q.; Shi, D.-X.; et al. Epitaxial Growth of Flat Antimonene Monolayer: A New Honeycomb Analogue of Graphene. *Nano Lett.* **2018**, *18*, 2133−2139.
(44) Wu, X.; Shao, Y.; Liu, H.; Feng, Z.; Wang, Y.-L.; Sun, J.-T.; Liu, C.; Wang, J.-O.; Liu, Z.-L.; Zhu, S.-Y.; et al. Epitaxial Growth and Air-Stability of Monolayer Antimonene on PdTe 2. *Adv. Mater.* **2017**, *29*, 1605407.
(45) Sun, S.; Yang, T.; Luo, Y. Z.; Gou, J.; Huang, Y.; Gu, C.; Ma, Z.; Lian, X.; Duan, S.; Wee, A. T. S.; et al. Realization of a Buckled Antimonene Monolayer on Ag(111) via Surface Engineering. *J. Phys. Chem. Lett.* **2020**, *11*, 8976−8982.
(46) Shi, Z.-Q.; Li, H.; Yuan, Q.-Q.; Song, Y.-H.; Lv, Y.-Y.; Shi, W.; Jia, Z.-Y.; Gao, L.; Chen, Y.-B.; Zhu, W.; et al. Van Der Waals Heteroepitaxial Growth of Monolayer Sb in a Puckered Honeycomb Structure. *Adv. Mater.* **2019**, *31*, 1806130.
(47) Aktürk, O. Ü.; Özçelik, V. O.; Ciraci, S. Single-Layer Crystalline Phases of Antimony: Antimonenes. *Phys. Rev. B* **2015**, *91*, 235446.
(48) Sun, X.; Song, Z.; Liu, S.; Wang, Y.; Li, Y.; Wang, W.; Lu, J. Sub-5 Nm Monolayer Arsenene and Antimonene Transistors. *ACS Appl. Mater. Interfaces* **2018**, *10*, 22363−22371.
(49) Yin, Y.; Shao, C.; Zhang, C.; Zhang, Z.; Zhang, X.; Robertson, J.; Guo, Y. Anisotropic Transport Property of Antimonene MOSFETs. *ACS Appl. Mater. Interfaces* **2020**, *12*, 22378−22386.
(50) Pizzi, G.; Gibertini, M.; Dib, E.; Marzari, N.; Iannaccone, G.; Fiori, G. Performance of Arsenene and Antimonene Double-Gate MOSFETs from First Principles. *Nat. Commun.* **2016**, *7*, 12585.
(51) Zhang, H.; Xiong, J.; Ye, M.; Li, J.; Zhang, X.; Quhe, R.; Song, Z.; Yang, J.; Zhang, Q.; Shi, B.; et al. Interfacial Properties of Monolayer Antimonene Devices. *Phys. Rev. Appl.* **2019**, *11*, No. 064001.
(52) Kresse, G.; Furthmüller, J. Efficient Iterative Schemes for *Ab Initio* Total-Energy Calculations Using a Plane-Wave Basis Set. *Phys. Rev. B* **1996**, *54*, 11169−11186.
(53) Perdew, J. P.; Burke, K.; Ernzerhof, M. Generalized Gradient Approximation Made Simple. *Phys. Rev. Lett.* **1996**, *77*, 3865−3868.
(54) Evarestov, R. A.; Smirnov, V. P. Modification of the Monkhorst-Pack Special Points Meshes in the Brillouin Zone for Density Functional Theory and Hartree-Fock Calculations. *Phys. Rev. B* **2004**, *70*, 233101.
(55) Momma, K.; Izumi, F. VESTA : A Three-Dimensional Visualization System for Electronic and Structural Analysis. *J. Appl. Crystallogr.* **2008**, *41*, 653−658.
(56) Grimme, S. Semiempirical GGA-Type Density Functional Constructed with a Long-Range Dispersion Correction. *J. Comput. Chem.* **2006**, *27*, 1787−1799.
(57) Wang, B.; Alhassan, S. M.; Pantelides, S. T. Formation of Large Polysulfide Complexes during the Lithium-Sulfur Battery Discharge. *Phys. Rev. Appl.* **2014**, *2*, No. 034004.
(58) Assary, R. S.; Curtiss, L. A.; Moore, J. S. Toward a Molecular Understanding of Energetics in Li−S Batteries Using Nonaqueous Electrolytes: A High-Level Quantum Chemical Study. *J. Phys. Chem. C* **2014**, *118*, 11545−11558.
(59) Barchasz, C.; Molton, F.; Duboc, C.; Leprêtre, J.-C.; Patoux, S.; Alloin, F. Lithium/Sulfur Cell Discharge Mechanism: An Original Approach for Intermediate Species Identification. *Anal. Chem.* **2012**, *84*, 3973−3980.
(60) Zhao, Y.; Yang, L.; Zhao, J.; Cai, Q.; Jin, P. How to Make Inert Boron Nitride Nanosheets Active for the Immobilization of Polysulfides for Lithium−Sulfur Batteries: A Computational Study. *Phys. Chem. Chem. Phys.* **2017**, *19*, 18208−18216.
(61) Qie, Y.; Liu, J.; Wang, S.; Gong, S.; Sun, Q. C3B Monolayer as an Anchoring Material for Lithium-Sulfur Batteries. *Carbon* **2018**, *129*, 38−44.
(62) Shao, Y.; Wang, Q.; Hu, L.; Pan, H.; Shi, X. $BC_2N$ Monolayers as Promising Anchoring Materials for Lithium-Sulfur Batteries: First-Principles Insights. *Carbon* **2019**, *149*, 530−537.


https://doi.org/10.1021/acs.energyfuels.1c00607
*Energy Fuels* 2021, 35, 9001−9009

(63) Wang, Y.; Ma, Z.; Song, N.; Zhang, T.; Zhang, Q.; Yang, D.; Wang, F. Metallic $VS_2$ Monolayer as an Anchoring Material for Lithium-Sulfur Batteries. *Chem. Phys. Lett.* **2020**, *741*, 137121.
(64) Xu, G.; Yan, Q.; Wang, S.; Kushima, A.; Bai, P.; Liu, K.; Zhang, X.; Tang, Z.; Li, J. A Thin Multifunctional Coating on a Separator Improves the Cyclability and Safety of Lithium Sulfur Batteries. *Chem. Sci.* **2017**, *8*, 6619−6625.
(65) Liao, K.; Mao, P.; Li, N.; Han, M.; Yi, J.; He, P.; Sun, Y.; Zhou, H. Stabilization of Polysulfides via Lithium Bonds for Li−S Batteries. *J. Mater. Chem. A* **2016**, *4*, 5406−5409.
(66) Wang, J.; Yang, H.; Chen, Z.; Zhang, L.; Liu, J.; Liang, P.; Yang, H.; Shen, X.; Shen, Z. X. Double-Shelled Phosphorus and Nitrogen Codoped Carbon Nanospheres as Efficient Polysulfide Mediator for High-Performance Lithium-Sulfur Batteries. *Adv. Sci.* **2018**, *5*, 1800621.
(67) Lin, H.; Yang, D.-D.; Lou, N.; Zhu, S.-G.; Li, H.-Z. Functionalized Titanium Nitride-Based MXenes as Promising Host Materials for Lithium-Sulfur Batteries: A First Principles Study. *Ceram. Int.* **2019**, *45*, 1588−1594.
(68) Zhao, J.; Yang, Y.; Katiyar, R. S.; Chen, Z. Phosphorene as a Promising Anchoring Material for Lithium−Sulfur Batteries: A Computational Study. *J. Mater. Chem. A* **2016**, *4*, 6124−6130.
(69) Liu, D.; Zhang, C.; Zhou, G.; Lv, W.; Ling, G.; Zhi, L.; Yang, Q.-H. Catalytic Effects in Lithium-Sulfur Batteries: Promoted Sulfur Transformation and Reduced Shuttle Effect. *Adv. Sci.* **2018**, *5*, 1700270.
(70) Xu, N.; Qian, T.; Liu, X.; Liu, J.; Chen, Y.; Yan, C. Greatly Suppressed Shuttle Effect for Improved Lithium Sulfur Battery Performance through Short Chain Intermediates. *Nano Lett.* **2017**, *17*, 538−543.


https://doi.org/10.1021/acs.energyfuels.1c00607
*Energy Fuels* 2021, 35, 9001−9009